Limits of realizing irradiance distributions with shift-invariant illumination systems and finite etendue sources

Heemels, Alexander N.M.; Adam, Aurele J.L.; Urbach, H. Paul

DOI
10.1364/JOSAA.488849

Publication date
2023

Document Version
Final published version

Published in
Journal of the Optical Society of America A: Optics and Image Science, and Vision

Citation (APA)
Heemels, A. N. M., Adam, A. J. L., & Urbach, H. P. (2023). Limits of realizing irradiance distributions with shift-invariant illumination systems and finite etendue sources. *Journal of the Optical Society of America A: Optics and Image Science, and Vision*, *40*(7), 1289-1302. https://doi.org/10.1364/JOSAA.488849

Research Article | Vol. 40, No. 7 / July 2023 / Journal of the Optical Society of America A | 1289

Journal of the Optical Society of America A
OPTICS, IMAGE SCIENCE, AND VISION

Limits of realizing irradiance distributions with shift-invariant illumination systems and finite étendue sources

Alexander N. M. Heemels,* Aurèle J. L. Adam, and H. Paul Urbach

Optics Research Group, Department of Imaging Physics, Delft University of Technology, Delft, The Netherlands
*a.n.m.heemels@tudelft.nl

Received 28 February 2023; revised 15 May 2023; accepted 15 May 2023; posted 16 May 2023; published 6 June 2023

When redistributing the light emitted by a source into a prescribed irradiance distribution, it is not guaranteed that, given the source and optical constraints, the desired irradiance distribution can be achieved. We analyze the problem by assuming an optical *black box* that is shift-invariant, meaning that a change in source position does not change the shape of the irradiance distribution, only its position. The irradiance distribution we can obtain is then governed by deconvolution. Using positive-definite functions and Bochner's theorem, we provide conditions such that the irradiance distribution can be realized for finite étendue sources. We also analyze the problem using optimization, showing that the result heavily depends on the chosen source distribution.

https://doi.org/10.1364/JOSAA.488849

1. INTRODUCTION

Optical designers and researchers have extensively studied the problem of designing an optical element that redistributes the light emitted by a source into a prescribed irradiance distribution. Numerous optical elements can be used to achieve this redistribution of light, such as freeform refractive and reflective optics [1–3], freeform gradient index lenses [4,5], micro-optics, and/or diffractive optical elements [6]. One common assumption to solve the problem is to design for zero-étendue sources, such as point sources or highly collimated sources, e.g., lasers. This assumption in most practical applications is too strict, as the size or divergence of the actual source is not negligible, and hence we have to design for a finite étendue source [7–10].

However, when solving this problem for finite étendue sources, there is no guarantee that the desired irradiance distribution is realizable with the given source. The issue of realizing an irradiance distribution with high spatial details with a finite étendue source can be discussed in terms of the resolution limits of freeform optical elements [11,12]. We further investigate whether a given finite étendue source can realize a specific irradiance distribution.

We assume an optical *black box* system that is shift-invariant, meaning that a shift in source position does not affect the shape of the distribution, only its position. Using this assumption, we can express the irradiance obtained from a finite étendue source as the convolution between the source and the zero-étendue response of the illumination system. Previous work has proposed formulating the design problem of a freeform for an extended source as a zero-étendue problem by deconvolving the desired irradiance with the blurring caused by the source [13–16]. However, the source extent's effect on the quality of the obtainable irradiance distributions has received limited attention. We investigate this relationship by taking inspiration from deblurring images in astronomy and microscopy [17] where prior information of the system response, such as nonnegativity and finite support, are used in an attempt to find a physically feasible blur kernel [18]. We use the definitions of positive definiteness and Bochner's theorem to analyze the problem and highlight the issues in realizing the desired irradiance distribution for simple sources. Furthermore, we show that restricting the point sources to be located in a grid with equal intensities can simplify the problem and help find analytic solutions. To conclude, we propose a method of approximating the irradiance with a basis of nonnegative functions and show that the approximation's quality of the desired irradiance distribution heavily depends on the chosen source for optimization. These results are then compared to regularization methods commonly used in the deblurring of images.

2. SHIFT-INVARIANT RESPONSE

To analyze the problem of which irradiance distributions can be realized with a finite étendue source, we consider an optical black box system that redirects the light emitted by a source on the optical axis into an irradiance distribution E_p, as seen in Fig. 1, which we call the optical impulse response of the system.

We assume that the system is shift-invariant, meaning that a source at position $\mathbf{r}^s$ in the source plane illuminating the optical

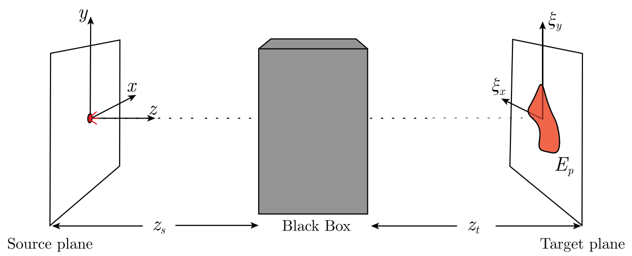

Fig. 1. Optical black box system redirects the light emitted by a point source on the optical axis located in the source plane to generate an irradiance distribution E_p, called the impulse response.

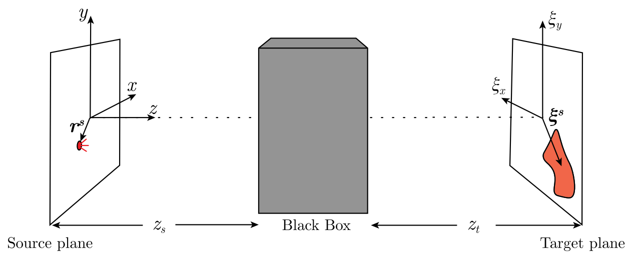

Fig. 2. Light emitted by a point source located at $\mathbf{r}^s$ in the source plane is redirected by the optical black box system to generate E_p, which is shifted by an amount $\boldsymbol{\xi}^s$ with $\boldsymbol{\xi}^s \propto \mathbf{r}^s$.

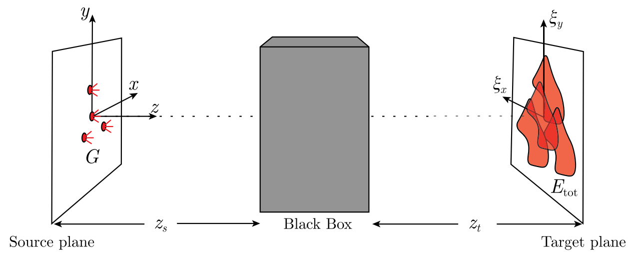

Fig. 3. Multiple point sources in the source plane give an irradiance distribution E_{tot}.

black box system will shift the impulse response by an amount $\boldsymbol{\xi}^s$ in the target plane directly proportional to $\mathbf{r}^s$, as depicted in Fig. 2.

Now consider a set of N_s mutually incoherent monochromatic sources emitting the same wavelength in the source plane at $\mathbf{r}_n^s$ each with a different intensity a_n. Then the total irradiance at the target plane E_{tot} is the incoherent sum of the contribution of each point source:

$$E_{\mathrm{tot}}(\boldsymbol{\xi}) = \iint E_p(\boldsymbol{\xi} - \boldsymbol{\xi}^s) G(\boldsymbol{\xi}^s) \mathrm{d}\boldsymbol{\xi}^s, \tag{1}$$

where G is the blurring caused by the source and is defined as

$$G(\boldsymbol{\xi}) = \sum_{n=1}^{N_s} a_n \delta(\boldsymbol{\xi}^s - \boldsymbol{\xi}_n^s). \tag{2}$$

Under this assumption, we can analyze the problem as a deconvolution problem where we want to find the impulse response E_p using a predefined irradiance distribution E_{tot} and source blurring G as depicted in Fig. 3.

3. REGULARIZED DECONVOLUTION OF TARGET DISTRIBUTION

Given a desired irradiance distribution E_{tot} and a source blur G, we want to find the impulse response of the optical black box system such that when illuminated with the given source, the desired irradiance distribution is obtained. All these functions are measures of radiometric energy. Hence they are nonnegative:

$$E_{\mathrm{tot}}(\boldsymbol{\xi}),\ E_p(\boldsymbol{\xi}),\ G(\boldsymbol{\xi}) \geq 0 \text{ for all } \boldsymbol{\xi} \in \mathbb{R}^2.$$

To find an E_p for a given source blur, the following minimizing problem has to be solved:

$$\min_{E_p} \| E_{\mathrm{tot}}(\boldsymbol{\xi}) - E_p(\boldsymbol{\xi}) * G(\boldsymbol{\xi}) \|_2^2, \tag{3}$$

where $\|\cdot\|_2$ is the L^2-norm. We use the Fourier transform, which we define as

$$\mathcal{F}\{f\}(\widehat{\boldsymbol{\xi}}) = \iint f(\boldsymbol{\xi}) \mathrm{e}^{-2\pi i \boldsymbol{\xi}\cdot\widehat{\boldsymbol{\xi}}} \mathrm{d}\boldsymbol{\xi}, \tag{4}$$

where $\widehat{\boldsymbol{\xi}}$ is the reciprocal coordinate of $\boldsymbol{\xi}$, and $\widehat{f}(\boldsymbol{\xi}) = \mathcal{F}\{f\}(\boldsymbol{\xi})$. The inverse Fourier transform is defined as

$$\mathcal{F}^{-1}\{f\}(\boldsymbol{\xi}) = \iint f(\widehat{\boldsymbol{\xi}}) \mathrm{e}^{2\pi i \boldsymbol{\xi}\cdot\widehat{\boldsymbol{\xi}}} \mathrm{d}\widehat{\boldsymbol{\xi}}. \tag{5}$$

A solution for E_p can then be found in Fourier space [19]:

$$E_p(\boldsymbol{\xi}) = \mathcal{F}^{-1}\left\{ \frac{\widehat{G}(\widehat{\boldsymbol{\xi}})\widehat{E}_{\mathrm{tot}}(\widehat{\boldsymbol{\xi}})}{|\widehat{G}(\widehat{\boldsymbol{\xi}})|^2 + \varepsilon} \right\}(\boldsymbol{\xi}), \tag{6}$$

where ε prevents division by zero. Using Eq. (6), let us look at the solution obtained when using the 1D rectangle function as the desired irradiance distribution:

$$E_{\mathrm{tot}}(\xi) = \mathrm{rect}\left(\frac{\xi_x}{\alpha}\right) \quad \text{with} \quad \mathrm{rect}\left(\frac{\xi_x}{\alpha}\right) \equiv \begin{cases} 1 & \text{if } |\xi_x| \leq \alpha, \\ 0 & \text{if } |\xi_x| > \alpha, \end{cases} \tag{7}$$

with two sources of equal strength. Figure 4(a0) shows the desired irradiance distribution $E_{\mathrm{tot}}(\xi_x) = \mathrm{rect}(\xi_x/0.5)$ with a source blur $G(\xi_x) = \delta(\xi_x + 0.25) + \delta(\xi_x - 0.25)$. $E_p(\xi_x)$ obtained from Eq. (6) with $\varepsilon = 10^{-14}$ is shown in Fig. 4(b0). It is a nonnegative function with bounded support. However, when we slightly change the width of E_{tot} to $\alpha = 0.51$ while keeping G unchanged, the obtained impulse response as seen in Fig. 4(b1) has negative values and does not have bounded support anymore. Something similar happens when leaving E_{tot} unchanged, and the source positions are slightly changed. As seen in Fig. 4(b2), this results in an E_p which oscillates rapidly, has no finite support, and has negative values.

From these results, it is clear that this problem is ill posed and is very sensitive to perturbations of the desired irradiance distribution and the a source blur. To better understand when a nonnegative E_p is obtained and what requirements should be imposed on E_{tot} and G to assure this, we can make use of *positive-definite functions* (Definition 1) and *Bochner's theorem* (Theorem 2).

Definition 1 (positive-definite functions) *A continuous function* $\Phi : \mathbb{R}^n \to \mathbb{C}$ *is positive definite on* $\mathbb{R}^n$ *if for every* $N \geq 1$ *and every* $\mathbf{x}_1, \ldots, \mathbf{x}_N \in \mathbb{R}^n$, *there holds*

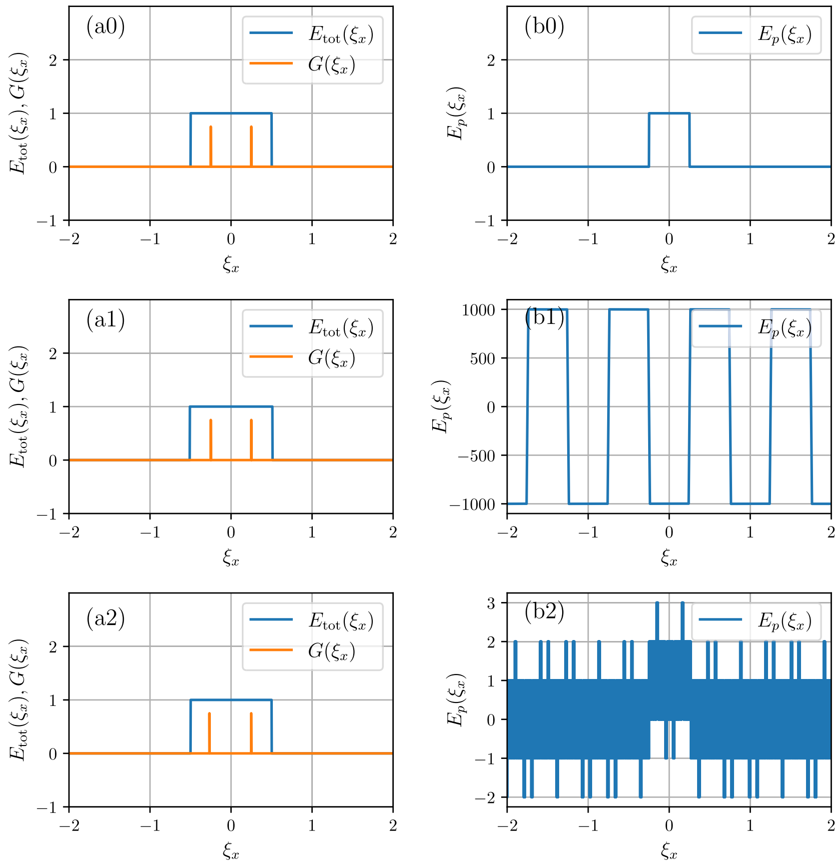

Fig. 4. Results from applying regularized deconvolution to a rectangular function when $\varepsilon = 10^{-14}$: (a0) $E_{\rm tot}(\xi_x) = {\rm rect}(\xi_x/0.5)$ and $G(\xi_x) = \delta(\xi_x + 0.25) + \delta(\xi_x - 0.25)$; (b0) $E_p(\xi_x)$; (a1) $E_{\rm tot}(\xi_x) = {\rm rect}(1.02\xi_x/0.51)$ and $G(\xi_x) = \delta(\xi_x + 0.25) + \delta(\xi_x - 0.25)$; (b1) $E_p(\xi_x)$; (a2) $E_{\rm tot}(\xi_x) = {\rm rect}(\xi_x/0.5)$ and $G(\xi_x) = \delta(\xi_x + 0.25) + \delta(\xi_x - 0.2501)$; (b2) $E_p(\xi_x)$. Results are obtained using linear sampling of ξ_x on the domain $[-5, 5]$ with $N = 1000001$ points.

$$\sum_{j=1}^{N} \sum_{k=1}^{N} c_j \bar{c}_k \Phi(\mathbf{x}_j - \mathbf{x}_k) \geq 0$$

for all complex numbers $[c_1, \ldots, c_N]^T \in \mathbb{C}$. *Hence the matrix with elements* $\Phi(x_j - x_k)$ *is hermitian and nonnegative.*

Theorem 1 (properties of positive-definite functions [20]**)**

(a) *Any nonnegative finite linear combination of a positive-definite function is positive definite, i.e., if* $\Phi_1, \ldots \Phi_m$ *are positive definite on* $\mathbb{R}^n$ *and* $w_j \geq 0$ *for all* $j = 1, \ldots, m$, *then*

$$\Phi(\mathbf{x}) = \sum_{j=1}^{m} w_j \Phi_j(\mathbf{x}), \quad \mathbf{x} \in \mathbb{R}^n$$

is also positive definite on $\mathbb{R}^n$.

(b) *For any positive-definite function,* $\Phi(\mathbf{0}) \geq 0$.

(c) *For any positive-definite function,* $\Phi(-\mathbf{x}) = \overline{\Phi(\mathbf{x})}$.

(d) *Any positive-definite function is bounded. In fact,*

$$|\Phi(\mathbf{x})| \leq \Phi(\mathbf{0}) \quad \text{for all } \mathbf{x} \in \mathbb{R}^n.$$

(e) *If* Φ *is positive definite with* $\Phi(\mathbf{0}) = 0$, *then* $\Phi = 0$.

(f) *The product of positive-definite functions is positive definite.*

Theorem 2 (Bochner's theorem [20]**)** *A (complex-valued) function* $\Phi \in C(\mathbb{R}^n)$ *is positive definite on* $\mathbb{R}^n$ *if and only if it is the Fourier transform of a bounded Borel measure* μ *on* $\mathbb{R}^n$, *i.e.,*

$$\Phi(\mathbf{x}) = \widehat{\mu}(\mathbf{x}) = \frac{1}{\sqrt{(2\pi)^n}} \int_{\mathbb{R}^n} e^{-i\mathbf{x}\cdot\mathbf{y}} \mathrm{d}\mu(\mathbf{y}), \quad \mathbf{x} \in \mathbb{R}^n.$$

Since functions $E_{\rm tot}$, K, and E_p are nonnegative, Bochner's theorem implies that Fourier transforms $\widehat{E}_{\rm tot}$, $\widehat{G}$, and $\widehat{E}_p$ are all positive definite. When applying regularized deconvolution of Eq. (6), we can use Property 1f: positive definiteness is preserved under multiplication. This property guarantees that $\widehat{E}_p$ is positive definite if $1/\widehat{G}$ is also positive definite but is not a necessary condition. It is simple to show that this cannot be the case because $\widehat{G}(\mathbf{0}) \geq |\widehat{G}(\widehat{\boldsymbol{\xi}})|$ for all $\widehat{\boldsymbol{\xi}} \in \mathbb{R}^2$ implies that $1/\widehat{G}(\mathbf{0}) \leq |1/\widehat{G}(\widehat{\boldsymbol{\xi}})|$ for all $\widehat{\boldsymbol{\xi}} \in \mathbb{R}^2$. Hence if $1/\widehat{G}$ were positive definite, $1/\widehat{G}(\mathbf{0}) \leq |1/\widehat{G}(\widehat{\boldsymbol{\xi}})| \leq 1/\widehat{G}(\mathbf{0})$, requiring $|\widehat{G}|$ to be constant, which is possible only when only a single source is used. Therefore, if multiple sources are used, it is not possible for $|\widehat{G}(\widehat{\boldsymbol{\xi}})|$ to be constant. Thus, $1/\widehat{G}$ is in general not positive definite, and hence $\widehat{E}_{\rm tot}/\widehat{G}$ is in general also not positive definite, and hence $\widehat{E}_p$ is not positive definite. Besides the single source solution, a second trivial case exists where $G(\boldsymbol{\xi}) = E_{\rm tot}(\boldsymbol{\xi})$ with $E_p(\boldsymbol{\xi}) = \delta(\boldsymbol{\xi})$. This case is realized by choosing the distribution

E_{tot} as the source and projecting it to the desired target plane using an imaging system.

One can view these two trivial solutions as two extreme solutions to the problem of realizing the desired irradiance using a combination of source and optical systems. The first solution corresponds to putting all the information into the optical system and using only a single source. In contrast, the second solution corresponds to shaping the source distribution and imaging it. The challenge is to find useful solutions between these two extremes. Therefore, we could reformulate the minimization described in Eq. (3) by treating both the blur and impulse response as variables leading to a blind deconvolution problem given by

$$\min_{E_p, G} \| E_{\text{tot}}(\boldsymbol{\xi}) - E_p(\boldsymbol{\xi}) * G(\boldsymbol{\xi}) \|_2^2 . \tag{8}$$

Algorithms such as iterative blind deconvolution [21] and Richardson–Lucy deconvolution [22–24] can then be used to find both the source and impulse response of the system. However, despite our efforts in applying these methods, they have yet to produce significant results. Therefore, we limit our analysis to cases where the source is given.

A. Analytic Example

To be able to analyze the problem with an analytic example, we impose a couple of restrictions on the source blur, given by Eq. (2) of which the Fourier transform is

$$\widehat{G}(\widehat{\boldsymbol{\xi}}) = \sum_{i=0}^{N_s} |a_i|^2 \exp(i\widehat{\boldsymbol{\xi}} \cdot \boldsymbol{\xi}_i). \tag{9}$$

The sum of complex exponentials can be rewritten as a complex function:

$$\widehat{G}(\widehat{\boldsymbol{\xi}}) = \left|\widehat{G}(\widehat{\boldsymbol{\xi}})\right| \exp(i\Phi_{\widehat{G}}(\widehat{\boldsymbol{\xi}})), \tag{10}$$

where $\Phi_{\widehat{G}}$ is the phase of the complex function, and $|\widehat{G}|$ is the modulus, which can be written as

$$|\widehat{G}(\widehat{\boldsymbol{\xi}})| = \sqrt{\sum_{n=0}^{N_s} a_n^2 + \sum_{n\neq m} 2a_n a_m \cos(\widehat{\boldsymbol{\xi}} \cdot (\boldsymbol{\xi}_n - \boldsymbol{\xi}_m))}, \tag{11}$$

$$\Phi_{\widehat{G}}(\widehat{\boldsymbol{\xi}}) = \arctan\left(\frac{\sum_{n=0}^{N_s} a_n \sin(\widehat{\boldsymbol{\xi}} \cdot \boldsymbol{\xi}_n)}{\sum_{n=0}^{N_s} a_n \cos(\widehat{\boldsymbol{\xi}} \cdot \boldsymbol{\xi}_n)}\right). \tag{12}$$

To obtain a valid solution, $\widehat{E}_{\text{tot}}/\widehat{G}$ should, according to Property 4.d, be bounded, which is the case when all the zeros of $|\widehat{G}|$ are also zeros of $\widehat{E}_{\text{tot}}$. However, $|\widehat{G}|$ is a cosine polynomial of which only a lower bound can be given for the number of zeros [25,26] making it extremely challenging to ensure that all the zeros are found. Two assumptions can be made to simplify Eqs. (11) and (12). The first assumes that all sources have the same intensity $a_n = a$ for all $n = 1, \ldots, N_s$. The second restricts the source positions to be equidistant with some separation $\Delta\boldsymbol{\xi} = [\Delta\xi_x, \ \Delta\xi_y]^T$, such that $\Delta\boldsymbol{\xi}_n = n\Delta\boldsymbol{\xi}$. Combining these assumptions gives the following expression for Eq. (9):

$$\widehat{G}(\widehat{\boldsymbol{\xi}}) = a \sum_{n=0}^{N_s} \exp\left(i\widehat{\boldsymbol{\xi}} \cdot n\Delta\boldsymbol{\xi}\right), \tag{13}$$

which can simplified to

$$\widehat{G}(\widehat{\boldsymbol{\xi}}) = a \frac{\sin(N_s\widehat{\boldsymbol{\xi}} \cdot \Delta\boldsymbol{\xi}/2)}{\sin(\widehat{\boldsymbol{\xi}} \cdot \Delta\boldsymbol{\xi}/2)} \exp(iN_s\widehat{\boldsymbol{\xi}} \cdot \Delta\boldsymbol{\xi}/2). \tag{14}$$

This expression is closely linked to the Dirichlet kernel [27], and it enables the analytical analysis of specific desired irradiance distributions.

Again consider the 1D rectangle function of Eq. (7) as the desired irradiance distribution; then its Fourier transform is

$$\widehat{E}_{\text{tot}}(\widehat{\xi}_x) = \frac{1}{a}\text{sinc}\left(\frac{\pi\widehat{\xi}_x}{a}\right) = \frac{\sin(\pi\widehat{\xi}_x/a)}{\pi\widehat{\xi}_x}. \tag{15}$$

We can calculate E_p using the simplified kernel Eq. (14):

$$\widehat{E}_p(\widehat{\xi}_x) = \frac{\sin(\pi\widehat{\xi}_x/a)}{\pi\widehat{\xi}_x} \frac{\sin(\widehat{\xi}_x\Delta\xi/2)}{\sin(N_s\widehat{\xi}_x\Delta\xi/2)} \times \exp(-i\widehat{\xi}_x\Delta\xi(N_s-1)/2). \tag{16}$$

By setting $\Delta\xi = 2\pi/N_s a$, the sine in the denominator is canceled by the fist sinus in the numerator, leaving us with

$$\widehat{E}_p(\widehat{\xi}_x) = \frac{1}{\pi\widehat{\xi}_x} \sin\left(\frac{\pi\widehat{\xi}_x}{N_s a}\right) \exp(-i\widehat{\xi}_x\widetilde{\Delta\xi}), \tag{17}$$

where $\widetilde{\Delta\xi} = \Delta\xi(N_s-1)/2$ is used to simplify the expression. We can rewrite this expression as a sinc function:

$$\widehat{E}_p(\widehat{\xi}_x) = \frac{1}{N_s a}\text{sinc}\left(\frac{\pi\widehat{\xi}_x}{N_s a}\right) \exp(-i\widehat{\xi}_x\widetilde{\Delta\xi}). \tag{18}$$

The inverse Fourier transform of Eq. (18) then gives the solution for the impulse response:

$$E_p(\xi_x) = \text{rect}\left(aN_s\xi_x - \widetilde{\Delta\xi}\right), \tag{19}$$

which is depicted in Fig. 5(b0). This expression shows that as the number of sources increases, an equal amount of rectangles can be placed next to each other to get back the original rectangle.

It should be noted that Eq. (19) is one of many solutions we can obtain. By rewriting Eq. (16) using the sine double angle formula, we can find

$$\widehat{E}_p(\widehat{\xi}_x) = \frac{2}{\pi\widehat{\xi}_x} \sin\left(\frac{\pi\widehat{\xi}_x}{2a}\right) \cos\left(\frac{\pi\widehat{\xi}_x}{2a}\right) \frac{\sin(\widehat{\xi}_x\Delta\xi/2)}{\sin(N_s\widehat{\xi}_x\Delta\xi/2)} \times \exp(-i\widehat{\xi}_x\Delta\xi(N_s-1)/2). \tag{20}$$

By choosing $\Delta\xi = \pi/(N_s a)$, the sinus in the denominator is canceled by the first sinus on the right-hand side of Eq. (20), and an alternative solution for the impulse response is obtained:

$$E_p(\xi_x) = \text{rect}\left(2N_s a\xi_x - \widetilde{\Delta\xi}\right) * \left[\delta\left(\xi_x + \frac{1}{4a}\right) + \delta\left(\xi_x - \frac{1}{4a}\right)\right]. \tag{21}$$

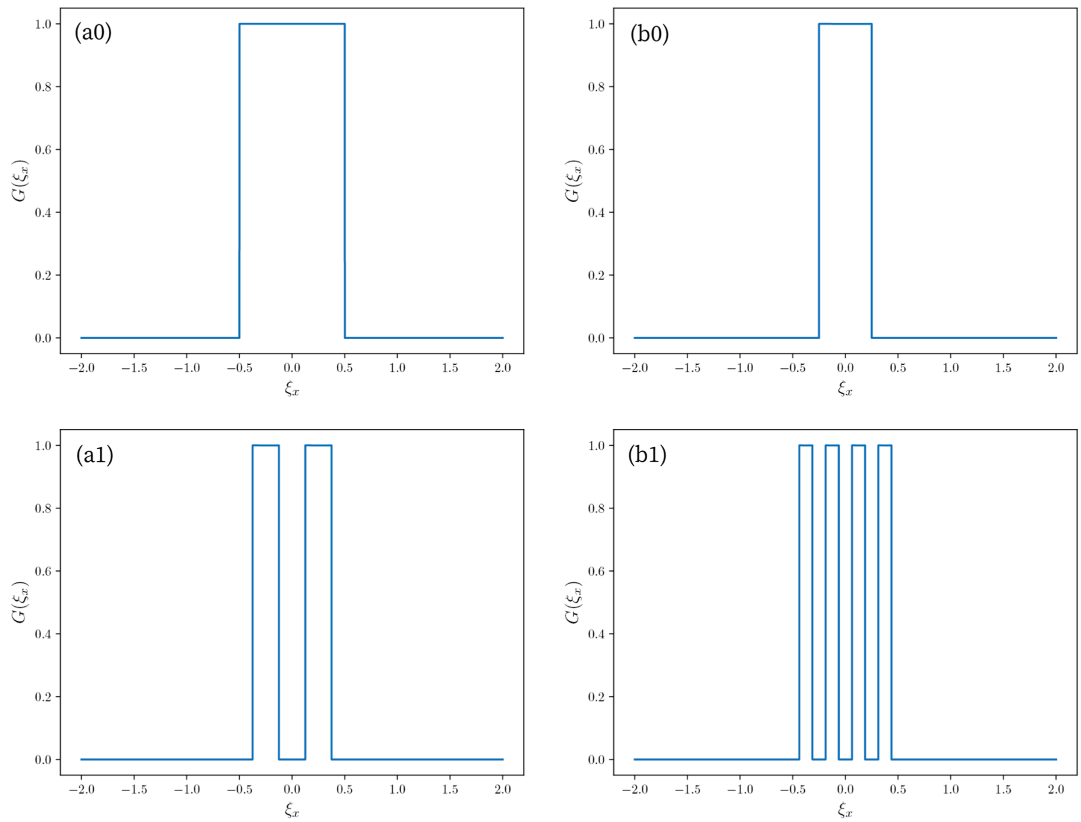

Fig. 5. Visualization of results obtained by applying Eqs. (19), (21), and (23) with $N_s = 2$: (a0) desired irradiance distribution; (b0) impulse response obtained using Eq. (19); (a1) impulse response obtained using Eq. (21); (b1) impulse response obtained using Eq. (23) with $M = 3$.

This solution can be understood as dividing the rectangle into $2N_s$ rectangles. The impulse response equals the combination of the first and the $(N_s + 1)^{\text{th}}$ rectangle, as seen in Fig. 5(a1).

The double angle formula can be applied an arbitrary number of times, and gives the general expression for when it is applied M times:

$$\widehat{E}_p(\widehat{\xi}_x) = \frac{2^M}{\pi\widehat{\xi}_x} \sin\left(\frac{\pi\widehat{\xi}_x}{2^M a}\right) \frac{\sin(\widehat{\xi}_x \Delta\xi/2)}{\sin(N_s\widehat{\xi}_x \Delta\xi/2)} \times \exp(-i\widehat{\xi}_x \Delta\xi(N_s - 1)/2) \prod_{m=1}^{M} \cos\left(\frac{\pi\widehat{\xi}_x}{2^m}\right). \tag{22}$$

By choosing $\Delta\xi = \pi/2^M N_s a$, the sinus in the denominator is again canceled. By Fourier transformation of the resulting expression, we get

$$E_p(\xi_x) = \text{rect}\big(2^M a\xi_x - \widetilde{\Delta\xi}\big) * \circledast_{m=1}^{M} \left[\delta\left(\xi_x + \frac{1}{2^{m+1}a}\right) + \delta\left(\xi_x - \frac{1}{2^{m+1}a}\right)\right]. \tag{23}$$

$\circledast_{m=1}^{M}$ is used to denote the M times repeated convolution:

$$f_1 * f_2 * \cdots * f_M = \circledast_{m=1}^{M} f_m. \tag{24}$$

This solution can be understood as dividing the rectangle into MN_s rectangles. The impulse response equals the combination of the first and every $(N_s + 1)^{\text{th}}$ rectangle after that; in Fig. 5(b2), the result is shown where the double sine angle is applied three times.

Based on this example, we can see the importance of correctly choosing the number of sources and the distance between them because, otherwise, the sines in Eq. (16) do not cancel. However, even with the assumptions used, finding an analytic expression for the impulse response E_p is possible only for a limited amount of cases. Therefore, estimating the desired irradiance distribution using a basis guaranteed to have a solution provides a more general approach.

4. APPROXIMATING THE IRRADIANCE DISTRIBUTION THROUGH OPTIMIZATION

As shown in Section 3.A, finding an analytic expression for the impulse response is possible only for a limited set of desired irradiance distributions. In addition, most irradiance distributions do not have an analytic expression, and we must turn to optimization to find a suitable E_p given an irradiance distribution E_{tot} and source blurring G.

To implement the minimization algorithm to solve Eq. (3), we formulate the discretized problem. Matrices $\mathbf{E}_{\text{tot}}$, $\mathbf{E}_p$, and $\mathbf{G}$ are the discrete counterparts of E_{tot}, E_p, and G and are matrices of dimension $N \times N$. Furthermore, to write Eq. (3) in terms of matrix and vector multiplications, we use the vectorization vec operator, which for the matrix

$$\mathbf{A}=\begin{bmatrix} a_{1,1} & a_{2,1} & \dots & a_{m,1} \\ a_{1,2} & a_{2,2} & \dots & a_{m,2} \\ \vdots & \ddots & \ddots & \vdots \\ a_{1,n} & a_{2,n} & \dots & a_{m,n} \end{bmatrix} \tag{25}$$

is defined as

$$\mathrm{vec}(\mathbf{A})=\left[a_{1,1},\ \dots,\ a_{m,1},\ a_{1,2},\ \dots,\ a_{m,2},\ a_{1,n},\ \dots\ a_{m,n}\right]^T. \tag{26}$$

In addition, we define the toeplitz operator for the general vector

$$\mathbf{a}=\left[a_1,\ a_2,\ a_3,\ \dots,\ a_{n-2},\ a_{n-1},\ a_n\right] \tag{27}$$

as

$$\mathrm{toepl}(\mathbf{a})=\begin{bmatrix} a_1 & 0 & \dots & 0 & 0 \\ a_2 & a_1 & \dots & 0 & 0 \\ \vdots & \vdots & \ddots & \vdots & \vdots \\ a_{n-1} & a_{n-2} & \ddots & a_1 & 0 \\ a_n & a_{n-1} & \ddots & a_2 & a_1 \end{bmatrix} \tag{28}$$

and the reshaping operator $\mathrm{resh}_{n\times m}$ as

$$\mathrm{resh}_{n\times m}(\mathbf{a})=\begin{bmatrix} a_1 & a_2 & \dots, & a_m \\ a_{m+1} & a_{m+2} & \dots, & a_{2m} \\ \vdots & \ddots & \ddots & \vdots \\ a_{(n-1)m+1} & a_{(n-1)m+2} & \dots & a_{nm} \end{bmatrix}, \tag{29}$$

which takes a vector of size NM and reshapes it into a matrix of size $N\times M$ such that for a square matrix $\mathbf{M}\in\mathbb{R}^{N\times N}$, we have $\mathbf{M}=\mathrm{resh}_{N\times N}(\mathrm{vec}(\mathbf{M}))$.

Using these operators, the convolution of two matrices can be written as a matrix vector multiplication:

$$\mathrm{vec}(\mathbf{G}*\mathbf{E}_p)=\mathrm{toepl}(\mathrm{vec}(\mathbf{G}))\mathrm{vec}(\mathbf{E}_p). \tag{30}$$

We can then formulate the discrete minimization problem as

$$\min_{\mathbf{E}_p}\left\|\mathrm{vec}(\mathbf{E}_{\mathrm{tot}})-\mathrm{toepl}[\mathrm{vec}(\mathbf{G})]\ \mathrm{vec}(\mathbf{E}_p)\right\|_2^2. \tag{31}$$

While solving Eq. (31), it is crucial to include prior information such as nonnegativity and finite support of the solution. To accomplish this, we describe two approaches: one involves approximating the desired irradiance distribution using nonnegative basis functions, while the other utilizes regularization techniques.

A. Approximation Using Nonnegative Basis Functions

We define a set of nonnegative functions $\{P_1,\ P_2,\ \dots,\ P_n\}$ with coefficient $\omega_i>0$ to approximate the distribution

$$E_{\mathrm{tot}}(\boldsymbol{\xi})\approx\sum_i \omega_i P_i(\boldsymbol{\xi})*G(\boldsymbol{\xi}),\quad \omega_i\ge 0. \tag{32}$$

Using this basis, we can then reformulate Eq. (3) as finding the optimal coefficients, such that the following expression is minimized:

$$\min_{\omega_1,\omega_2,\dots,\omega_n}\left\|E_{\mathrm{tot}}(\boldsymbol{\xi})-\sum_i G(\boldsymbol{\xi})*\omega_i P_i(\boldsymbol{\xi})\right\|_2^2. \tag{33}$$

Distribution E_p is then obtained by summing the weighted basis functions:

$$E_p(\boldsymbol{\xi})=\sum_i \omega_i P_i(\boldsymbol{\xi}). \tag{34}$$

A suitable choice for P is any probability distribution with finite support such as beta distributions, Bates distributions, Irwin distributions, or Kronecker delta distributions [28]. There are two ways of forming a basis for a chosen distribution. First, probability density functions defined by shape parameters, such as the beta distribution with shape parameters α and β,

$$P(x)=x^{\alpha-1}(1-x)^{\beta-1},\quad \alpha,\beta\ge 0\quad \text{and}\quad 0\ge x\ge 1, \tag{35}$$

allow for creating a non-orthogonal basis by choosing a range over which to define α and β and discretize it. For instance, select the range $\alpha\in[0,\ A]$ and $\beta\in[0,\ B]$ and the amount of functions in the set using N_α and N_β. Then the following set of basis functions is obtained:

$$P_{i,j}(x)=x^{iA/N_\alpha-1}(1-x)^{jB/N_\beta-1},\quad \text{with}\quad i=0,1,\dots,N_\alpha \quad \text{and}\quad j=0,1,\dots,N_\beta. \tag{36}$$

Second, a probability density function $P(x)$ that does not have shape parameters, such as Irwan–Hall distributions, can give a basis by spatially shifting $P(x)$ over a distance x_i by which the basis function becomes

$$P_i(x)=P(x)*\delta(x-x_i). \tag{37}$$

To obtain the discrete optimization problem, we define matrix $\mathbf{P}\in\mathbb{R}^{N^2\times M}$ as the concatenation of vectorized basis functions:

$$\mathbf{P}=\left[\mathrm{vec}(\mathbf{P}_1),\ \mathrm{vec}(\mathbf{P}_2),\ \dots,\ \mathrm{vec}(\mathbf{P}_M)\right], \tag{38}$$

and then $\mathrm{vec}(\mathbf{E}_p)$ can be calculated as

$$\mathrm{vec}(\mathbf{E}_p)=\mathbf{P}\boldsymbol{\omega}, \tag{39}$$

where $\boldsymbol{\omega}\in\mathbb{R}^{M\times 1}$ is a vector containing the weights of the basis functions. Combining Eqs. (31) and (39), the discrete minimization problem becomes

$$\min_{\boldsymbol{\omega}}\left\|\mathrm{vec}(\mathbf{E}_{\mathrm{tot}})-\mathrm{toepl}[\mathrm{vec}(\mathbf{G})]\ \mathbf{P}\boldsymbol{\omega}\right\|_2^2\quad \text{subject to}\quad \boldsymbol{\omega}\ge 0, \tag{40}$$

which can be solved using nonnegative least squares [29,30]. Once a $\boldsymbol{\omega}$ is found that minimizes Eq. (40) or a maximum number of iterations is reached, $\mathbf{E}_p$ can be calculated as

$$\mathbf{E}_p=\mathrm{resh}_{N\times N}\left(\mathbf{P}\,\boldsymbol{\omega}\right). \tag{41}$$

B. Regularized Optimization

Using prior information, we can constrain the optimization using a regularization term $R(\mathbf{E}_p)$, which is added to the loss function and can be added to Eq. (31) giving

$$\min_{\mathbf{E}_p} \left\| \mathrm{vec}(\mathbf{E}_{\mathrm{tot}}) - \mathrm{toepl}[\mathrm{vec}(\mathbf{G})]\mathrm{vec}(\mathbf{E}_p) \right\|_2^2 + \mu R(\mathbf{E}_p), \quad (42)$$

where μ is a weighting factor indicating the importance of the regularization term which can be used to enforce smoothness and nonnegativity. The most well known is *Thikonov regularization* [31], which sets the regulation factor to

$$R(\mathbf{E}_p) = \|\mathbf{L}\,\mathrm{vec}(\mathbf{E}_p)\|_2^2, \quad (43)$$

where $\mathbf{L}$ is a filter that penalizes a certain aspect of E_p. Often $\mathbf{L}$ is taken as the identity matrix, in which case the optimization is constrained such that the L^2-norm of $\mathrm{vec}(\mathbf{E}_p)$ does not become too large. Alternatively, $\mathbf{L}$ can be chosen as a discrete approximation of a derivative operator, in which case the smoothness of the solution is enforced. An alternative regulation term that is often used to enforce positivity is *maximum entropy regularization* [32,33], in which case the regularization term is given by

$$R(\mathbf{E}_p) = \sum_{i,j} \mathbf{E}_p(i,j) \log[\mathbf{E}_p(i,j)]. \quad (44)$$

5. RESULTS

We consider the case of two sources with equal intensity, yielding the following source blur:

$$G(\boldsymbol{\xi}) = \delta(\boldsymbol{\xi}) + \delta(\boldsymbol{\xi} + \boldsymbol{\Delta\xi}). \quad (45)$$

One source is fixed at the center of the source plane such that $\boldsymbol{\xi}^s = 0$, while the other can move freely with a position $\boldsymbol{\Delta\xi}$. A schematic representation is shown in Fig. 6.

For all cases, the target irradiance distribution is chosen to be of size 256×256, and the basis chosen for optimization consists of shifted Kronecker delta functions:

$$\delta(\boldsymbol{\xi}, \boldsymbol{\xi}_0) = \begin{cases} 0, & \text{if } \boldsymbol{\xi} \neq \boldsymbol{\xi}_0 \\ 1, & \text{if } \boldsymbol{\xi} = \boldsymbol{\xi}_0 \end{cases}. \quad (46)$$

The position of the second source is incrementally changed for source positions $\boldsymbol{\Delta\xi} = (m\Delta\xi_x, n\Delta\xi_y)$ with

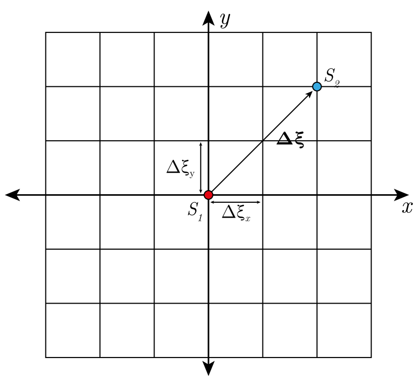

Fig. 6. Schematic representation of how the two sources are defined: the first source is located at the origin (on the optical axis), and the second has position vector $\boldsymbol{\Delta\xi} = (m\Delta\xi_x, n\Delta\xi_y)$.

$m, n \in [0, 20]$ and $\Delta\xi_x, \Delta\xi_y = 1/128$. The size of $\mathbf{G}$ becomes very large. However, due to the choice of source blur, the matrix $\mathrm{toepl}(\mathrm{vec}(\mathbf{G}))$ has only $2N^2$ non-zero elements allowing the use of sparsity. At each position, Eq. (3) is solved using nonnegative least squares, which is stopped once a maximum amount of iterations has exceeded or has not decreased for several iterations, yielding a solution for $E_p(\boldsymbol{\xi})$. The final L^2-norm value is stored in a matrix of size 20×20, called the loss matrix, and when plotted, shows a grid of the loss values, called the loss landscape. The loss landscape visualizes how well the optimization converges for the different source configurations.

The optimization was done for two desired irradiance distributions: a uniform square and a uniform circle, of which the results can be seen in Figs. 7 and 8, respectively.

The loss landscape of the uniform square distribution, Fig. 7(b0), shows several positions where good estimation is achieved, which are situated along the x and y axes. The impulse responses obtained for two cases are shown in Figs. 7(b1) and 7(b3). These solutions are equivalent to the analytical solutions found by applying the double sine formula in Eq. (23) in the x or y direction. Moving the source away from the x or y axis causes a degradation of the quality of the obtained irradiation distribution. The obtained distribution is shown in Figs. 7(a2) and 8(b2), the respective impulse response.

For the uniform circle, we see that the desired distribution can be accurately estimated when the distance between the two sources is small compared to the distribution size, as seen in Fig. 8(a1). As the distance between the sources increases, the estimation quality further degrades.

In all results, we see that if the shift induced by moving the source is small with respect to the size of the target irradiation distribution, an impulse response can be found, which can be used to approximate the desired distribution accurately.

A. Comparison with Regularization

We compare the results of the nonnegative basis function approximation with three types of regularization: maximum entropy, Tikhonov regularization with $\mathbf{L}$ the identity operator, and Tikhonov regularization with $\mathbf{L}$ the discrete Laplace operator, which is commonly used in edge detection [34] and is chosen to enforce smoothness of the solution and dampen out the wild oscillation observed in Figs. 4(b1) and 4(b2). We solved the regularized problems using *Regularization Tools* [35] employing different solvers for the regularized problems. The *maxent* solver was used to solve for the maximum entropy regularization, the conjugate gradient algorithm (*cgls*) for the Thikonov with identity regularization, and the preconditioned conjugate gradient algorithm (*pcgls*) for the discrete Laplace operator regularization. We compare the results of two sets of source positions for both square and circular distributions. For square distribution, we compare the results for source positions $\boldsymbol{\Delta\xi} = (8\Delta\xi_x, 0)$ (Fig. 9) and $\boldsymbol{\Delta\xi} = (6\Delta\xi_x, 6\Delta\xi_y)$ (Fig. 10). For circular distribution, we compare the results of source positions $\boldsymbol{\Delta\xi} = (0\Delta\xi_x, 4\Delta\xi_y)$ (Fig. 11) and $\boldsymbol{\Delta\xi} = (13\Delta\xi_x, 4\Delta\xi_y)$ (Fig. 12). For both cases of square distribution, the regularization parameter used to solve the maximum entropy was set to $\mu = 0.4642$. Both the preconditioned and regular conjugate

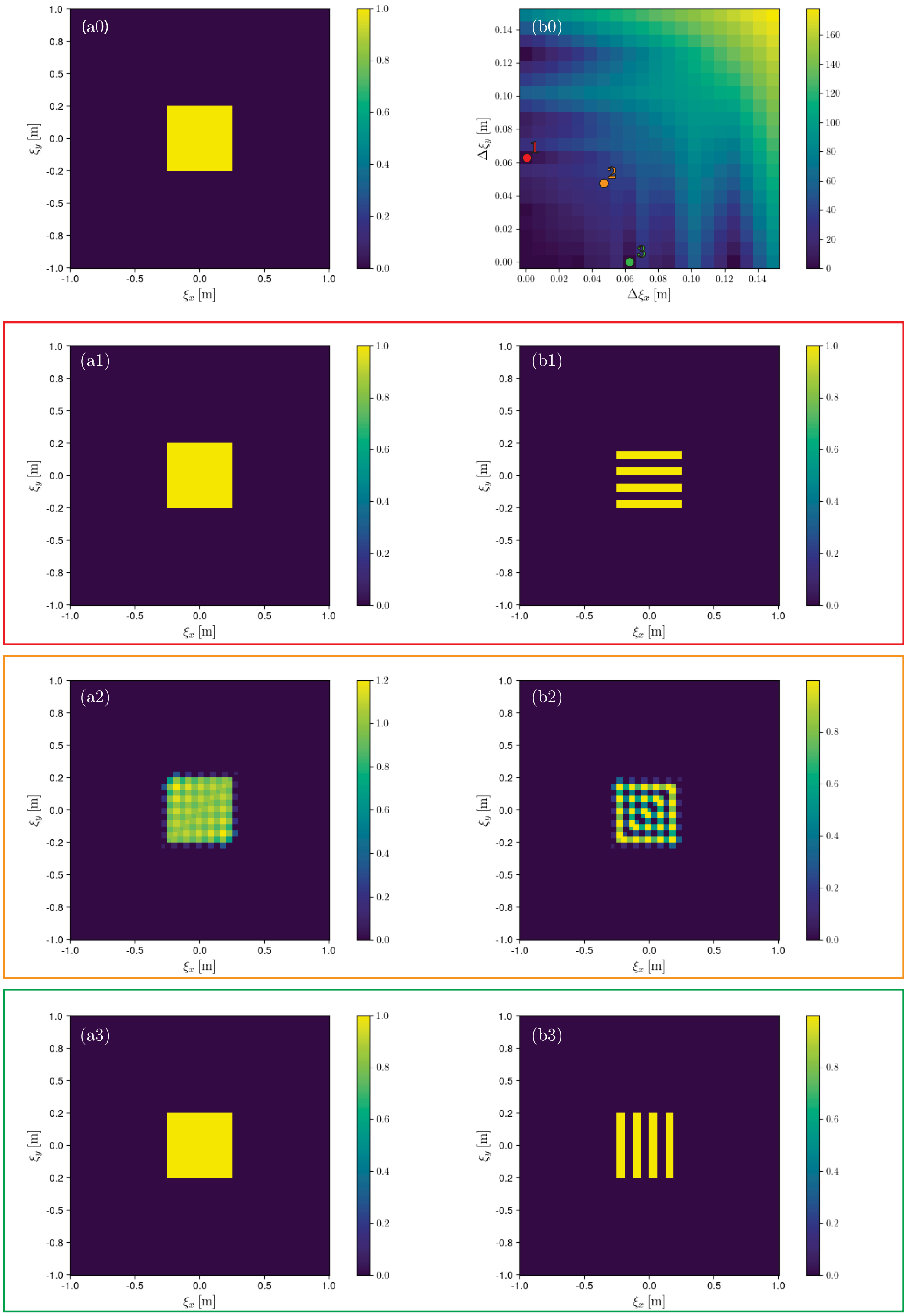

Fig. 7. (a0) Desired irradiance distribution: square distribution of width 0.5; (b0) loss landscape. (a1), (b1) Total irradiance and impulse response obtained for $\boldsymbol{\Delta\xi} = (0, 8\Delta\xi_y)$ (red dot). (a2), (b2) Total irradiance and impulse response obtained for $\boldsymbol{\Delta\xi} = (6\Delta\xi_x, 6\Delta\xi_y)$ (orange dot). (a3), (b3) Total irradiance and impulse response obtained for $\boldsymbol{\Delta\xi} = (8\Delta\xi_x, 0)$ (green dot).

gradient algorithms converged in 50 iterations. For circular distribution, $\mu = 0.315$ was chosen for the maximum entropy algorithm, and the preconditioned and regular conjugate gradient algorithms converged in 150 iterations.

In all test cases, the maximum entropy regularization produced nonnegative impulse responses and total irradiances, which, upon visual inspection, closely resembled the outcomes obtained through approximation by nonnegative basis functions. The results obtained using the conjugate gradient method converge to the known nonnegative solution as seen in Figs. 9(a1) and 9(b1). However, in all other scenarios, the obtained impulse response oscillates rapidly between positive

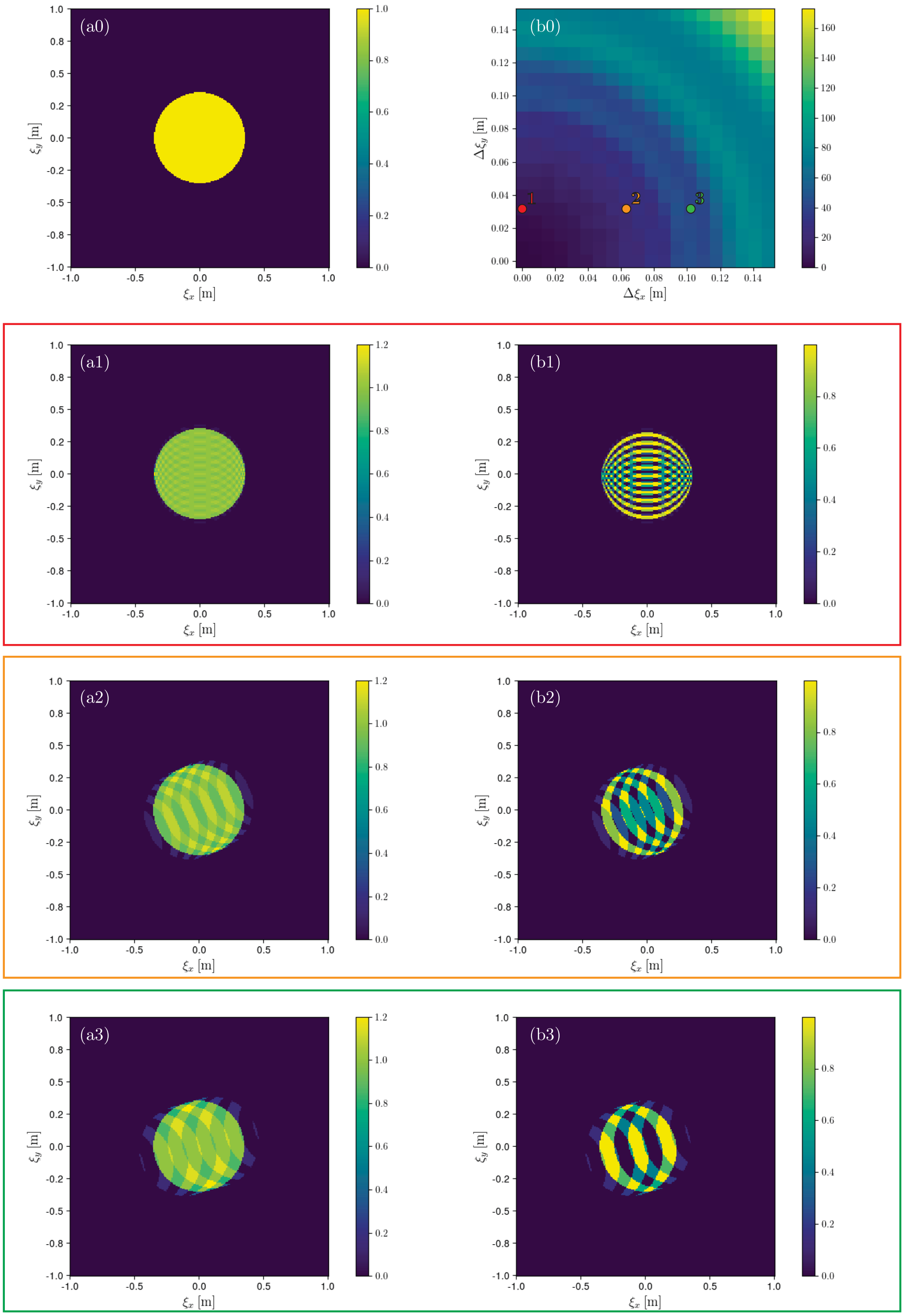

Fig. 8. (a0) Desired irradiance distribution: uniform circular distribution with radius 0.33; (b0) loss landscape. (a1), (b1) Total irradiance and impulse response obtained for $\mathbf{\Delta\xi} = (0, 4\Delta\xi_y)$ (red dot). (a2), (b2) Total irradiance and impulse response obtained for $\mathbf{\Delta\xi} = (8\Delta\xi_x, 4\Delta\xi_y)$ (orange dot). (a3), (b3) Total irradiance and impulse response obtained for $\mathbf{\Delta\xi} = (13\Delta\xi_x, 4\Delta\xi_y)$ (green dot).

and negative values and lacks finite support, as depicted in Figs. 10(b2), 11(b2), and 12(b2). Furthermore, the impulse responses obtained using the preconditioned conjugate gradient method with the discrete Laplace operator are much smoother than the other results, as shown in Figs. 10(b2), 11(b2), and 12(b2). Although both impulse response and total irradiance become negative, the amount is much less than the results obtained using the regular conjugate gradient algorithm.

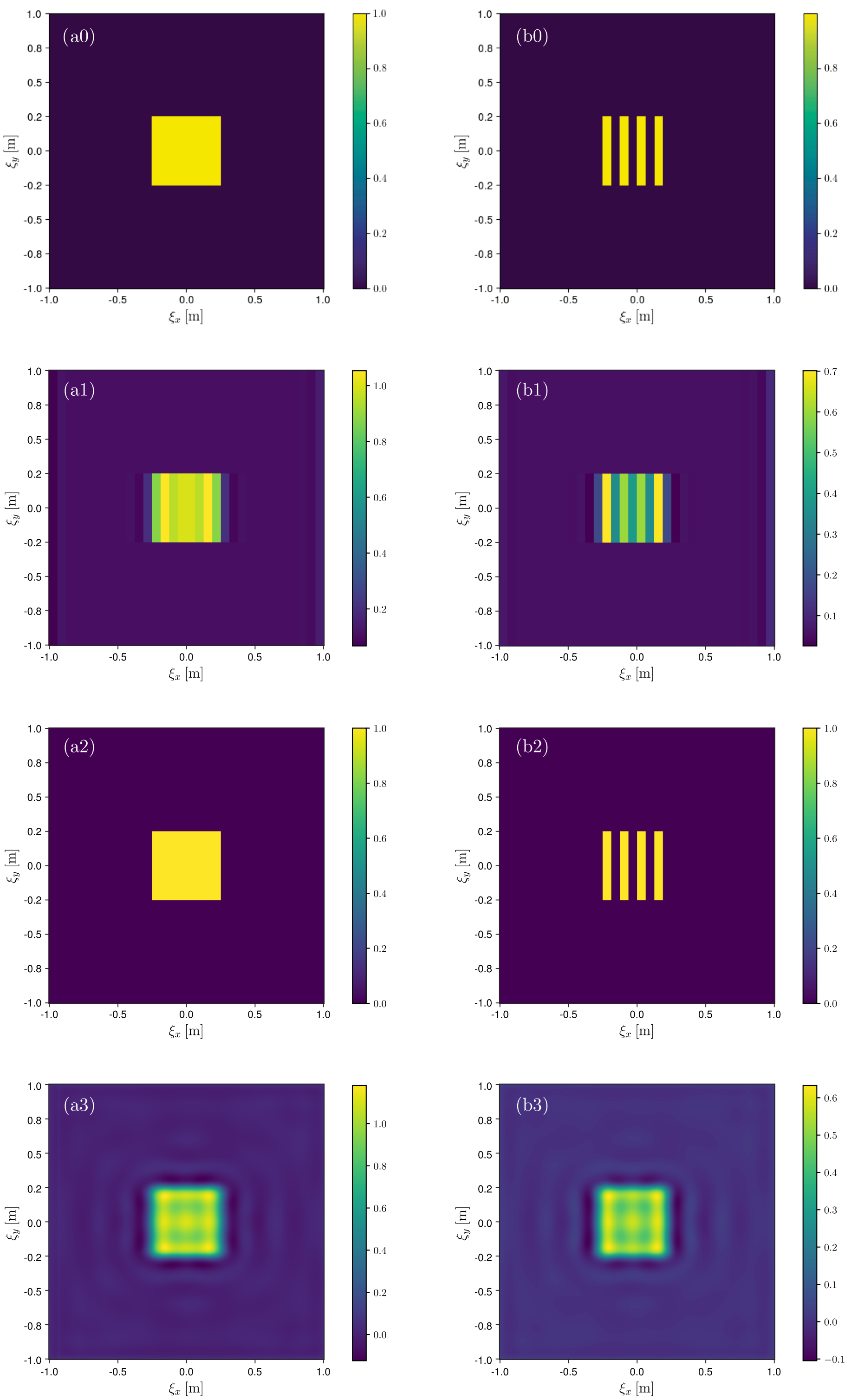

Fig. 9. Comparison of regularized results and approximation using nonnegative basis functions for square distribution and for $\boldsymbol{\Delta\xi} = (8\Delta\xi_x, 0)$. Total irradiances (left) and impulse responses (right) obtained using: (a0), (b0) approximation using nonnegative basis functions; (a1), (b1) maximum entropy regularization; (a2), (b2) conjugate gradient algorithm; (a3), (b3) preconditioned conjugate gradient algorithm and $\mathbf{L}$ the discrete Laplace operator.

Moreover, while the preconditioned conjugated gradient result extends beyond the desired irradiance domain, the oscillation appears to be damped towards the edges.

6. CONCLUSION

We have presented a mathematical study of the problem of generating a desired irradiance distribution under the assumption

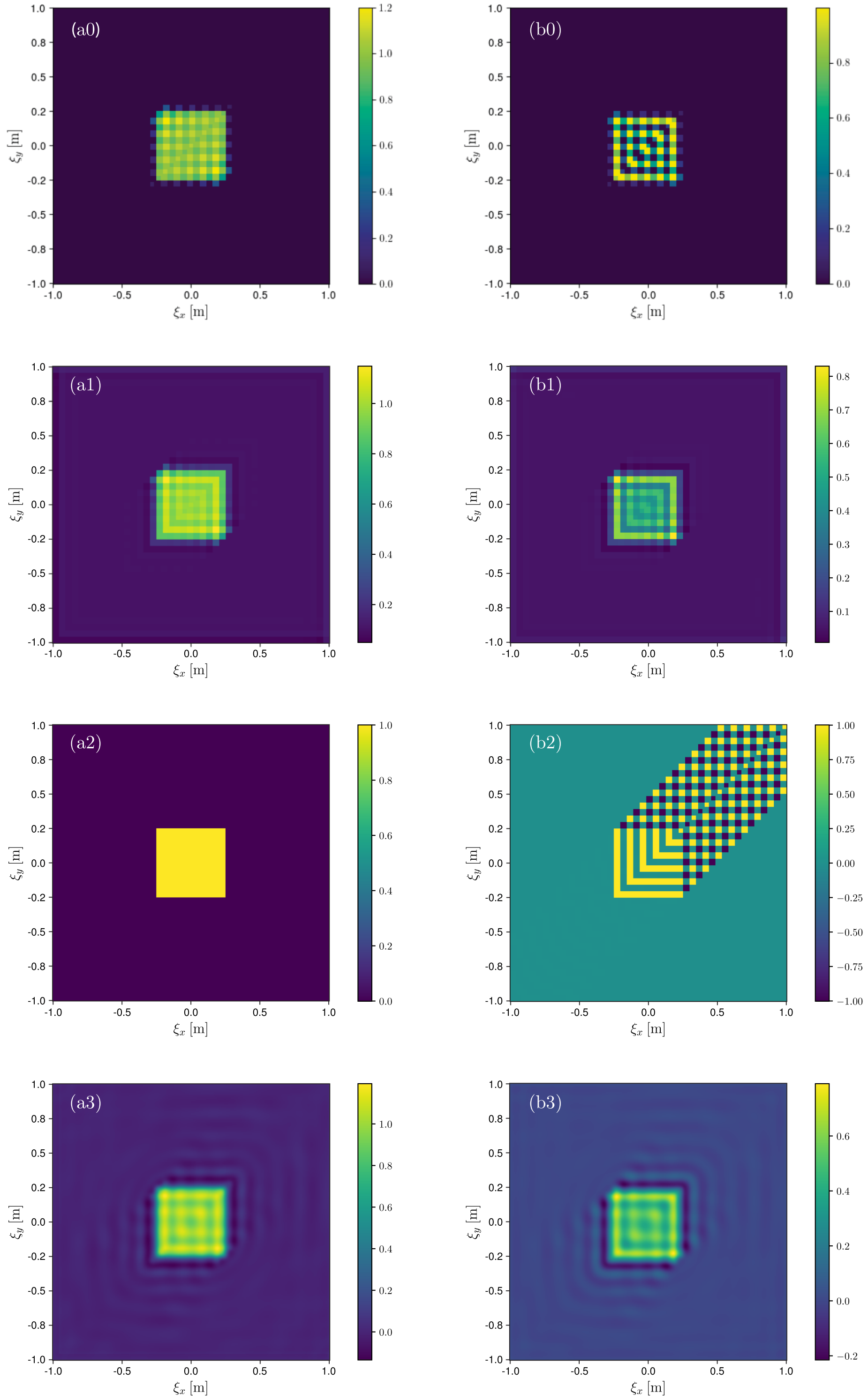

Fig. 10. Comparison of regularized results and approximation using nonnegative basis functions for square distribution and for $\boldsymbol{\Delta\xi} = (6\Delta\xi_x, 6\Delta\xi_y)$. Total irradiances (left) and impulse responses (right) obtained using: (a0), (b0) approximation using nonnegative basis functions; (a1), (b1) maximum entropy regularization; (a2), (b2) conjugate gradient algorithm; (a3), (b3) preconditioned conjugate gradient algorithm and $\mathbf{L}$ the discrete Laplace operator.

that the irradiance distributions generated by different point sources are the same except for a translation. This assumption can be analyzed as a deconvolution problem where the desired irradiance distribution, illumination, and impulse response should all be nonnegative. Using positive-definite functions and Bochner's theorem, we have shown two trivial solutions: one uses a single, zero-étendue source; the other shapes the source to be the desired irradiance distribution and designs an imaging

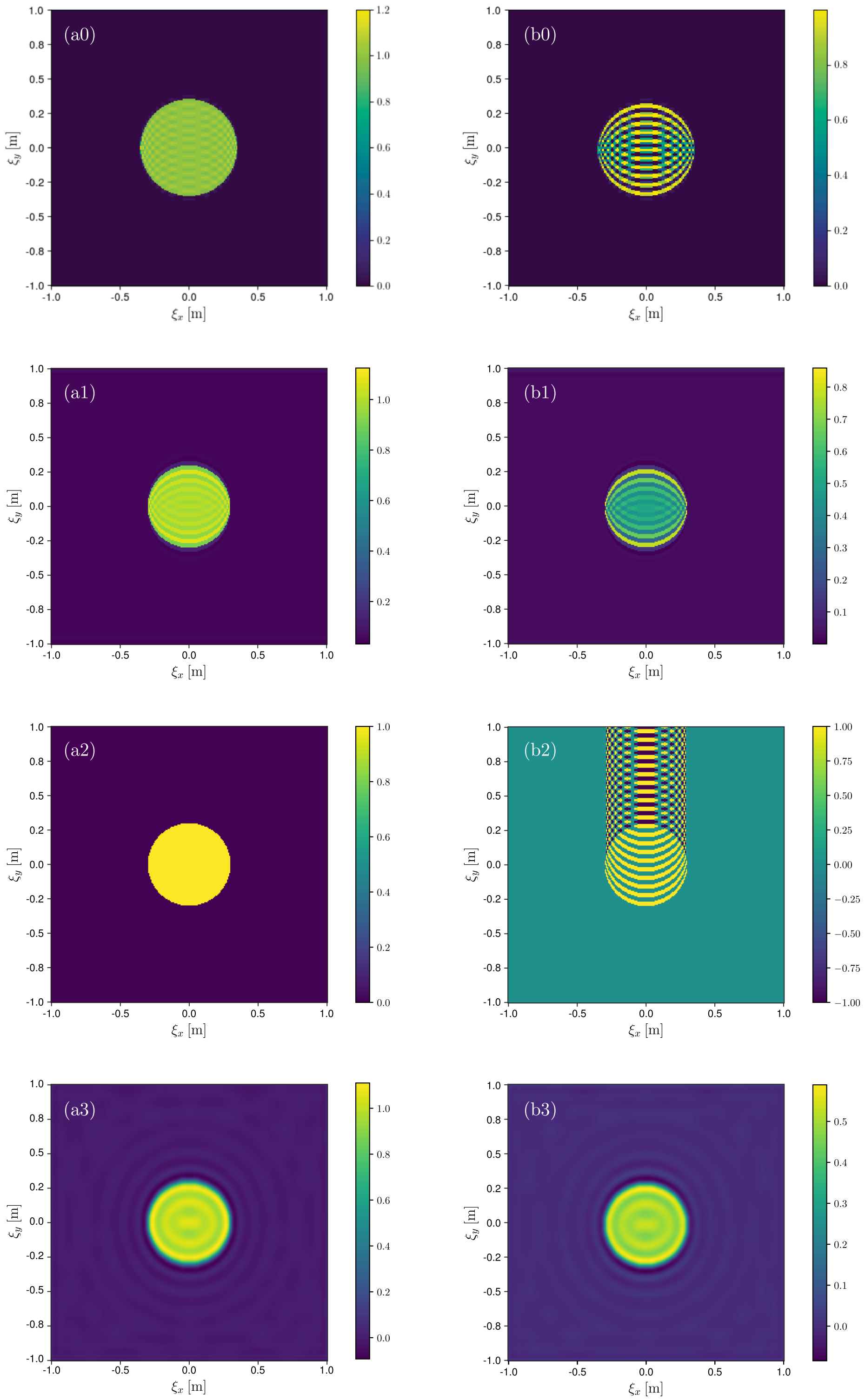

Fig. 11. Comparison of regularized results and approximation using nonnegative basis functions for circular distribution and for $\mathbf{\Delta \xi} = (0\Delta\xi_x, 4\Delta\xi_y)$. Total irradiances (left) and impulse responses (right) obtained using: (a0), (b0) approximation using nonnegative basis functions; (a1), (b1) maximum entropy regularization; (a2), (b2) conjugate gradient algorithm; (a3), (b3) preconditioned conjugate gradient algorithm and $\mathbf{L}$ the discrete Laplace operator.

system that projects it to the desired plane. When restricted to equidistantly spaced sources with equal strength, an analytic solution for E_p can be found in specific cases. However, a more general approach is obtained through optimization using a set of nonnegative basis functions. Analysis of the results showed, for the case of two sources, that if the shift induced by moving the source is small compared to the size of the irradiance distribution, a good estimation can be obtained. However, once this

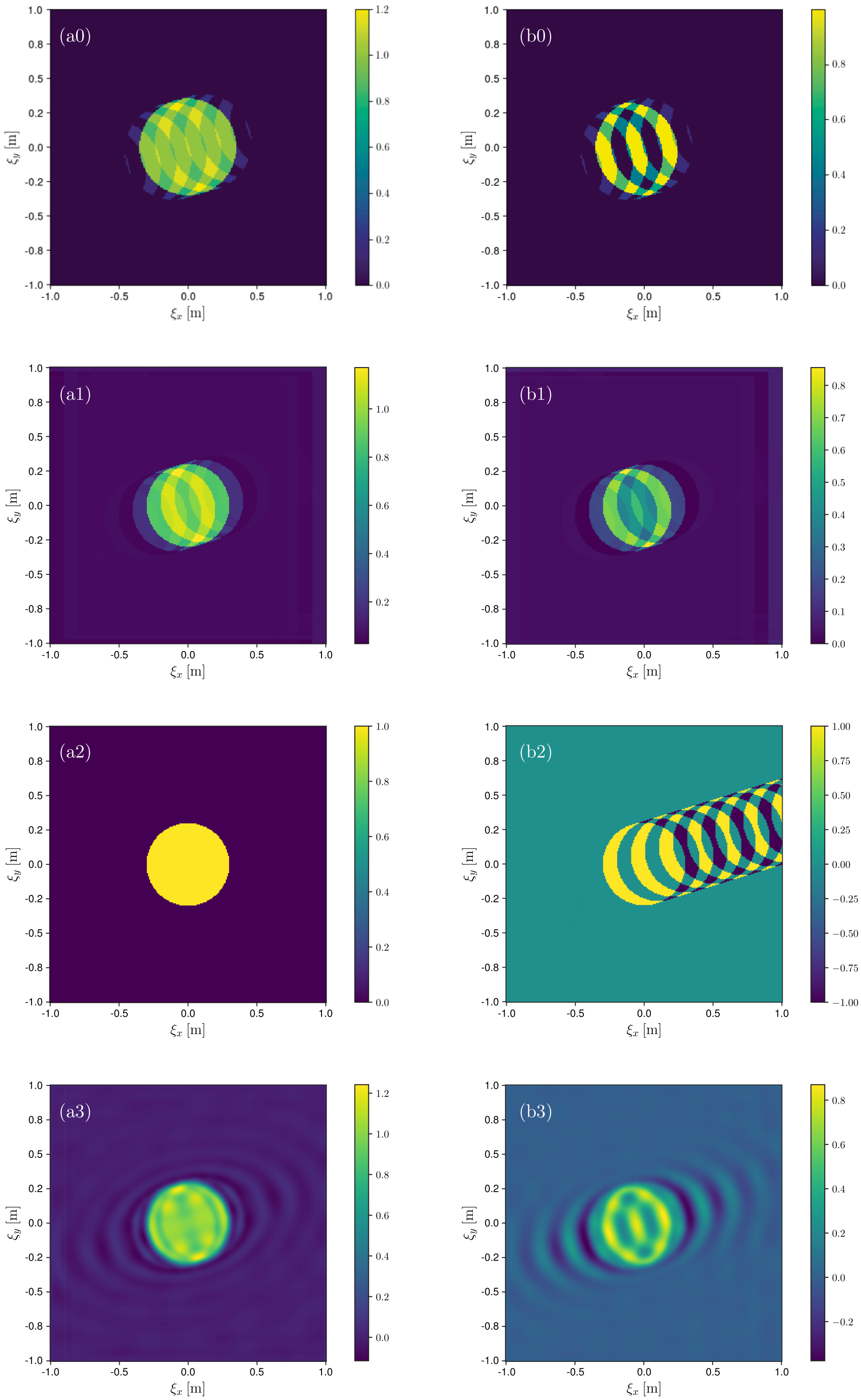

Fig. 12. Comparison of regularized results and approximation using nonnegative basis functions for circular distribution and for $\boldsymbol{\Delta\xi} = (13\Delta\xi_x, 4\Delta\xi_y)$. Total irradiances (left) and impulse responses (right) obtained using: (a0), (b0) approximation using nonnegative basis functions; (a1), (b1) maximum entropy regularization; (a2), (b2) conjugate gradient algorithm; (a3), (b3) preconditioned conjugate gradient algorithm and $\mathbf{L}$ the discrete Laplace operator.

shift becomes too large, the quality by which the desired irradiance distribution can be estimated decreases with the distance between sources.

We compared these results with various types of regularization. The maximum entropy regularization can come close to the solutions obtained by our proposed method. However, this approach requires careful selection of the regularization parameter to achieve optimal results. The conjugate gradient was able to converge to the known nonnegative solution. However, for all other cases, it converges to a solution that is neither nonnegative nor has finite support. Finally, the preconditioned gradient method with a discrete Laplace operator always converges to a solution that has negative values, but due to the smoothness constraint imposed by the Laplace operator, it has finite support but extends beyond the domain on which the desired irradiance distribution is defined.

Future work will address two crucial aspects. First, the issue of large matrices required to solve the problem will be tackled, enabling the analysis of higher-resolution irradiance and complex source distributions. Second, the theory should be extended to accommodate shift-variant impulse responses, which provide a more realistic representation of what is observed when moving a source in illumination systems.

Funding. Nederlandse Organisatie voor Wetenschappelijk Onderzoek (P15-36) "Free-form scattering optics."

Disclosures. The authors declare no conflicts of interest.

Data availability. Data underlying the results presented in this paper are not publicly available at this time but may be obtained from the authors upon reasonable request.

REFERENCES

1. H. Ries and J. Muschaweck, "Tailored freeform optical surfaces," J. Opt. Soc. Am. A **19**, 590–595 (2002).
2. M. J. H. Anthonissen, L. B. Romijn, J. H. M. ten Thije Boonkkamp, and W. L. Ijzerman, "Unified mathematical framework for a class of fundamental freeform optical systems," Opt. Express **29**, 31650–31664 (2021).
3. L. A. Caffarelli and V. I. Oliker, "Weak solutions of one inverse problem in geometric optics," J. Math. Sci. **154**, 39–49 (2008).
4. D. H. Lippman and G. R. Schmidt, "Prescribed irradiance distributions with freeform gradient-index optics," Opt. Express **28**, 29132–29147 (2020).
5. W. Minster Kunkel and J. R. Leger, "Numerical design of three-dimensional gradient refractive index structures for beam shaping," Opt. Express **28**, 32061–32076 (2020).
6. F. M. Dickey, ed., *Laser Beam Shaping: Theory and Techniques*, 2nd ed. (CRC Press, 2014).
7. M. Brand and D. A. Birch, "Freeform irradiance tailoring for light fields," Opt. Express **27**, A611–A619 (2019).
8. S. Sorgato, J. Chaves, H. Thienpont, and F. Duerr, "Design of illumination optics with extended sources based on wavefront tailoring," Optica **6**, 966–971 (2019).
9. J. A. Muschaweck, "Tailored freeform surfaces for illumination with extended sources," Proc. SPIE **12220**, 1222004 (2022).
10. F. R. Fournier, W. J. Cassarly, and J. P. Rolland, "Designing freeform reflectors for extended sources," Proc. SPIE **7423**, 742302 (2009).
11. S. Zwick, R. Feßler, J. Jegorov, and G. Notni, "Resolution limitations for tailored picture-generating freeform surfaces," Opt. Express **20**, 3642–3653 (2012).
12. M. Brand, "Minimum spot size and maximum detail in extended-source freeform illumination," in *OSA Optical Design and Fabrication 2021 (Flat Optics, Freeform, IODC, OFT)* (Optica, 2021), paper JTh1A.1.
13. D. Ma, Z. Feng, and R. Liang, "Deconvolution method in designing freeform lens array for structured light illumination," Appl. Opt. **54**, 1114–1117 (2015).
14. M. Brand and A. Aksoylar, "Sharp images from freeform optics and extended light sources," in *Frontiers in Optics* (Optica, 2016), paper FW5H.2.
15. A. Aksoylar, "Modeling and model-aware signal processing methods for enhancement of optical systems," Ph.D. dissertation (Boston University, 2016).
16. S. Wei, Z. Zhu, W. Li, and D. Ma, "Compact freeform illumination optics design by deblurring the response of extended sources," Opt. Lett. **46**, 2770–2773 (2021).
17. P. Campisi and K. Egiazarian, *Blind Image Deconvolution: Theory and Applications* (CRC Press, 2017).
18. A. S. Carasso, "False characteristic functions and other pathologies in variational blind deconvolution. a method of recovery," SIAM J. Appl. Math. **70**, 1097–1119 (2009).
19. E. Pantin, J.-L. Starck, and F. Murtagh, "Deconvolution and blind deconvolution in astronomy," in *Blind Image Deconvolution*, 1st ed. (CRC Press, 2007), pp. 277–316.
20. G. E. Fasshauer, *Meshfree Approximation Methods with MATLAB*, Interdisciplinary Mathematical Sciences (World Scientific, 2007), Vol. **6**.
21. G. Ayers and J. C. Dainty, "Iterative blind deconvolution method and its applications," Opt. Lett. **13**, 547–549 (1988).
22. L. B. Lucy, "An iterative technique for the rectification of observed distributions," Astron. J. **79**, 745–754 (1974).
23. W. H. Richardson, "Bayesian-based iterative method of image restoration," J. Opt. Soc. Am. **62**, 55–59 (1972).
24. D. A. Fish, A. M. Brinicombe, E. R. Pike, and J. G. Walker, "Blind deconvolution by means of the Richardson–Lucy algorithm," J. Opt. Soc. Am. A **12**, 58–65 (1995).
25. P. Borwein, T. Erdélyi, R. Ferguson, and R. Lockhart, "On the zeros of cosine polynomials: solution to a problem of Littlewood," Ann. Math. **167**, 1109–1117 (2008).
26. J. Sahasrabudhe, "Counting zeros of cosine polynomials: on a problem of Littlewood," Adv. Math. **343**, 495–521 (2019).
27. A. Bashirov, "Fourier series and integrals," in *Mathematical Analysis Fundamentals*, A. Bashirov, ed. (Elsevier, 2014), Chap. 12, pp. 307–345.
28. N. L. Johnson, S. Kotz, and N. Balakrishnan, *Continuous Univariate Distributions*, 2nd ed., Wiley Series in Probability and Mathematical Statistics (Wiley, 1994).
29. J. Nocedal and S. J. Wright, *Numerical Optimization*, Springer Series in Operations Research (Springer, 1999).
30. W. Forst and D. Hoffmann, *Optimization-Theory and Practice*, Springer Undergraduate Texts in Mathematics and Technology (Springer, 2010).
31. A. N. Tikhonov and V. Y. Arsenin, *Solutions of Ill-Posed Problems* (V. H. Winston & Sons; Wiley, 1977).
32. U. Amato and W. Hughes, "Maximum entropy regularization of Fredholm integral equations of the first kind," Inverse Probl. **7**, 793 (1991).
33. C. R. Smith and W. T. Grandy, Jr., *Maximum-Entropy and Bayesian Methods in Inverse Problems* (Springer, 2013), Vol. **14**.
34. P. A. Mlsna and J. J. Rodríguez, "Gradient and Laplacian edge detection," in *The Essential Guide to Image Processing*, A. Bovik, ed. (Academic, 2009), Chap. 19, pp. 495–524.
35. P. C. Hansen, "Regularization tools: a MATLAB package for analysis and solution of discrete ill-posed problems," Numer. Algorithms **6**, 1–35 (1994).